THE JOURNAL OF BIOLOGICAL CHEMISTRY VOL. 283, NO. 33, pp. 22858–22866, August 15, 2008

Structure of Human Cytosolic X-prolyl Aminopeptidase

A DOUBLE Mn(II)-DEPENDENT DIMERIC ENZYME WITH A NOVEL THREE-DOMAIN SUBUNIT[*][S]

Received for publication, December 18, 2007, and in revised form, April 23, 2008 Published, JBC Papers in Press, May 30, 2008, DOI 10.1074/jbc.M710274200

Xin Li[‡§], **Zhiyong Lou**[¶], **Xuemei Li**[§], **Weihong Zhou**[‡], **Ming Ma**[§], **Youjia Cao**[‡1], **Yunqi Geng**[‡], **Mark Bartlam**[‡¶], **Xuejun C. Zhang**[§‖2], **and Zihe Rao**[‡§¶]

From the [‡]*College of Life Sciences & Tianjin State Laboratory of Protein Sciences, Nankai University, Tianjin 300071, China, the* [§]*National Laboratory of Biological Macromolecules, Institute of Biophysics (IBP), Chinese Academy of Sciences, Beijing 100101, China, the* [¶]*Laboratory of Structural Biology, Tsinghua University, Beijing 100084, China, and the* [‖]*Crystallography Research Program, Oklahoma Medical Research Foundation, Oklahoma City, Oklahoma 73104*

X-prolyl aminopeptidases catalyze the removal of a penultimate prolyl residue from the N termini of peptides. Mammalian X-prolyl aminopeptidases are shown to be responsible for the degradation of bradykinin, a blood pressure regulator peptide, and have been linked to myocardial infarction. The x-ray crystal structure of human cytosolic X-prolyl aminopeptidase (XPNPEP1) was solved at a resolution of 1.6 Å. The structure reveals a dimer with a unique three-domain organization in each subunit, rather than the two domains common to all other known structures of X-prolyl aminopeptidase and prolidases. The C-terminal catalytic domain of XPNPEP1 coordinates two metal ions and shares a similar fold with other prolyl aminopeptidases. Metal content analysis and activity assays confirm that the enzyme is double Mn(II) dependent for its activity, which contrasts with the previous notion that each XPNPEP1 subunit contains only one Mn(II) ion. Activity assays on an E41A mutant demonstrate that the acidic residue, which was considered as a stabilizing factor in the protonation of catalytic residue His^{498}, plays only a marginal role in catalysis. Further mutagenesis reveals the significance of the N-terminal domain and dimerization for the activity of XPNPEP1, and we provide putative structural explanations for their functional roles. Structural comparisons further suggest mechanisms for substrate selectivity in different X-prolyl peptidases.

X-prolyl aminopeptidases (aminopeptidase P or AP-P; E.C. 3.4.11.9) are found in a variety of organisms including mammals, yeasts, and bacteria. There are two forms of mammalian AP-P in terms of their cellular locations: a cytosolic form (XPNPEP1) and a membrane-bound form (XPNPEP2). Both forms can degrade bradykinin, a blood pressure-regulating peptide, and are inhibited by the specific peptide inhibitor apstatin (1–3). The cytosolic form of AP-P has been identified in human leukocytes (4), platelets (5), and rat and guinea pig brains (6, 7). The membrane-bound form, first purified from porcine kidney (8) and later purified from bovine and rat lungs (1, 9), is attached to the lipid bilayer through a glycosylphosphatidylinositol anchor (10). A previous study has shown that injection of apstatin into mice can reduce myocardial infarction severity (11), suggesting a pathological role of X-prolyl aminopeptidases in mammals.

Human XPNPEP1 consists of 623 amino acid residues with a calculated molecular mass of 69,886 Da. The enzyme purified from human leukocytes exists as a dimer of 140 kDa (4). The catalytic activity of the enzyme is enhanced in the presence of Mn^{2+} (3). Each 70-kDa subunit of the enzyme was thought to contain only one Mn^{2+} ion in a previous study (3). A Blast search against the NCBI sequence data base revealed similarity in the C-terminal catalytic domains among X-prolyl peptidases of known structures. In contrast, the overall sequence homology between human XPNPEP1 and other X-prolyl peptidases is low. In particular, XPNPEP1 is significantly larger in size than other members of the X-prolyl peptidases (about 40–50 kDa).

Here we report the crystal structure of human XPNPEP1 at 1.6-Å resolution. Whereas other X-prolyl peptidases with known structures all contain two domains, the XPNPEP1 structure possesses a novel three-domain organization with a conserved C-terminal catalytic domain. In contrast to previous reports, we identified the presence of a double Mn^{2+} binding site in the catalytic domain, both in the crystal structure and in solution.

EXPERIMENTAL PROCEDURES

Cloning and Expression—The cDNA of wild type (WT) XPNPEP1 and that of a domain I-truncated mutant (residues 162–623) were cloned into the pET28a vector (Novagen) between SalI and HindIII sites. E41A (*i.e.* Glu^{41} to Ala substitution) and W477E point mutants were produced from the constructed pET28a-wild type XPNPEP1 plasmid with a one-step overlap extension PCR method by using the Easy Mutagenesis System kit (Transgen).

All XPNPEP1 variants were expressed as an N-terminal His_6-tagged protein in *Escherichia coli* BL21(DE3) in LB medium supplemented with 1 mM $MnCl_2$ (manganese-rich LB). Sel-

* This work was supported by Ministry of Science and Technology of China Grant 2006DFB32420, National 973 Program Grant 2007CB914301, and the Natural National Science Foundation of China Grant 30221003. The costs of publication of this article were defrayed in part by the payment of page charges. This article must therefore be hereby marked "*advertisement*" in accordance with 18 U.S.C. Section 1734 solely to indicate this fact.
[S] The on-line version of this article (available at http://www.jbc.org) contains supplemental Figs. S1 and S2 and Table S1.
[1] To whom correspondence may be addressed. E-mail: caoyj@nankai.edu.cn.
[2] To whom correspondence may be addressed. E-mail: Cai-Zhang@omrf.org.

enomethionine-substituted WT[3] protein was expressed in a *metE*$^-$ *E. coli* host strain B834 (Novagen) in the M9 minimal medium supplemented with 50 mg of selenomethionine per liter and 1 mM $MnCl_2$.

For expression, *E. coli* cells cultured overnight were diluted 100-fold in fresh medium and cultured at 37 °C to an optical density of about 0.8 at 600 nm. The cell culture was then cooled down to 16 °C and induced with 0.5 mM isopropyl β-D-1-thiogalactopyranoside. It was grown for another 20 h at 16 °C with shaking at 220 rpm, and then the cells were harvested by centrifugation.

Protein Purification—The harvested cells were resuspended in buffer A (20 mM Tris-HCl (pH 7.9), 500 mM NaCl, and 10% (v/v) glycerol) and lysed by sonication. The released His_6-tagged protein was purified following standard protocols of nickel-nitrilotriacetic acid resin (Qiagen). It was eluted from the resin with buffer B (20 mM Tris-HCl (pH 7.9), 500 mM NaCl, 10% (v/v) glycerol, and 300 mM imidazole) and dialyzed against a salt-free buffer (20 mM Tris-HCl (pH 8.0)). Further purification was performed with a Hitrap Q HP affinity column (Amersham Biosciences) and the final protein sample was dialyzed against a buffer of 20 mM Tris-HCl (pH 8.0) and 20 mM NaCl.

Crystallization—Crystals of native or selenomethionyl-labeled protein were grown by the hanging-drop vapor-diffusion method. The reservoir contained 20% (v/v) polyethylene glycol (PEG) 400, 0.15 M $CaCl_2$, and 100 mM HEPES (pH 7.5). A typical hanging drop consisted of 2 μl of protein solution (20 mg/ml) mixed with 2 μl of the reservoir solution. Large (over 0.5 mm) colorless block-shaped crystals suitable for diffraction were grown within a week at 16 °C.

Data Collection, Phasing, and Model Refinement—Crystallographic data from the crystals of native and selenomethionyl-labeled protein were collected on beamlines BL5A and BL17A of the Photon Factory synchrotron facility (KEK, Tsukuba, Japan). The diffraction images were integrated and scaled using HKL2000 (12). A 3.5-Å resolution structure of selenomethionyl-labeled XPNPEP1 was solved by the multiwavelength anomalous diffraction phasing method at the selenium absorption edge using SOLVE/RESOLVE (13). The 3.5-Å resolution phases were extended to 1.6 Å using the native data set and the program ARP/WARP (14). The program automatically built about 80% of residues, and the remainder were built manually with COOT (15). The structure was refined with REFMAC5 (16). Figures were drawn with the program PYMOL (DeLano Scientific, San Carlos, CA).

Enzyme Activity Assays—The enzyme activity was assayed with bradykinin (Phoenix Pharmaceuticals, Inc.) or the Arg-Pro-Pro tripeptide (synthesized by SBS Genetech, Beijing, China) as the substrate in 100 mM Tris-HCl (pH 8.0) and 100 mM NaCl at 37 °C for 5 min (100 μl final volume). The free amino acid released by the enzyme was detected with the *o*-phthalaldehyde, 5-mercaptoethanol reagent as previously described (9). Fluorescence of the *o*-phthalaldehyde derivate was measured with a microplate reader (Type 374, Thermo Electron Corporation). For kinetic analysis, assays were prepared with a range of concentrations of bradykinin (0.01–0.10 mM) or Arg-Pro-Pro (0.02–0.20 mM) and 1 μg of the purified WT enzyme. To examine the effects of different factors on the enzyme activity, 0.09 mM Arg-Pro-Pro and 1 μg of purified enzyme variant were used in a 100-μl assay. To verify the effect of EDTA, purified WT enzyme was incubated in 100 mM Tris-HCl (pH 8.0) and 100 mM NaCl with 50 mM EDTA for 10 min, and dialyzed against 100 mM Tris-HCl (pH 8.0) and 100 mM NaCl prior to measuring its relative activity.

Other Assays—Analysis of the total metal content was carried out using inductively coupled plasma mass spectrometry (ICP-MS, Thermo) at the Tsinghua University Analysis Center (Beijing, China). Purified protein samples without crystallization trial were extensively dialyzed against 100 mM Tris-HCl (pH 8.0) and 100 mM NaCl before ICP-MS analysis.

Analytical ultracentrifugations (AUC) were performed with the sedimentation velocity method at 58,000 rpm at the Institute of Biophysics, Chinese Academy of Sciences (Beijing, China). The protein samples for AUC were prepared at a concentration of about 0.5 mg/ml in a buffer of 100 mM Tris-HCl (pH 8.0) and 100 mM NaCl. The AUC data were processed as a c(M) distribution model (17).

RESULTS

Structure Determination and Refinement—The structure of human XPNPEP1 was solved at 1.6-Å resolution using the multiwavelength anomalous diffraction method. Refinement of the XPNPEP1 structure resulted in a final model with a crystallographic *R*-factor (R_{cryst}) of 0.154 and a free *R*-factor (R_{free}) of 0.195. One asymmetric unit of this $C222_1$ crystal form contained a single protein molecule composed of 623 amino acid residues. The polypeptide chain was complete with the exception of the N-terminal His_6 tag, the N-terminal residues 1–2, and the C-terminal residues 620–623, which were not included in the final model because of poor electron density. For the same reason, Asn^{553}, Arg^{554}, and the side chain of Phe^{509} were assigned zero occupancy. All other residues had excellent electron density, and the final average temperature factor (*B*) was 27.2 $Å^2$. An asymmetric unit also contained 1,055 ordered water molecules, one partial PEG molecule containing six ethylene glycol residues, and four metal ions. Of the four metal ions, two major ones localized at the active site were refined as full occupancy Mn^{2+} with temperature factors of 14.8 $Å^2$ (Mn1 in Fig. 1*A*) and 17.7 $Å^2$ (Mn2), respectively. The two minor ions were refined as full occupancy Ca^{2+} and Na^+, respectively. Although crystals were grown in 0.15 M $CaCl_2$, native XPNPEP1 treated with EDTA (followed by dialysis before crystallization) yielded no crystal but thick precipitation under the same condition, suggesting that the two active-site metal ions observed in the native crystal protein were unlikely to be calcium ions replacing Mn^{2+} during crystallization. Besides the mobile Asn^{553}, only Glu^{434}, affected by the inter-molecule Ca^{2+}, localizes in the Ramachandran unfavorable region. Experimental structure factors and the coordinates of the refined model have been deposited in the Protein Data

[3] The abbreviations used are: WT, wild type; ICP-MS, inductively coupled plasma mass spectrometry; AUC, analytical ultracentrifugation.

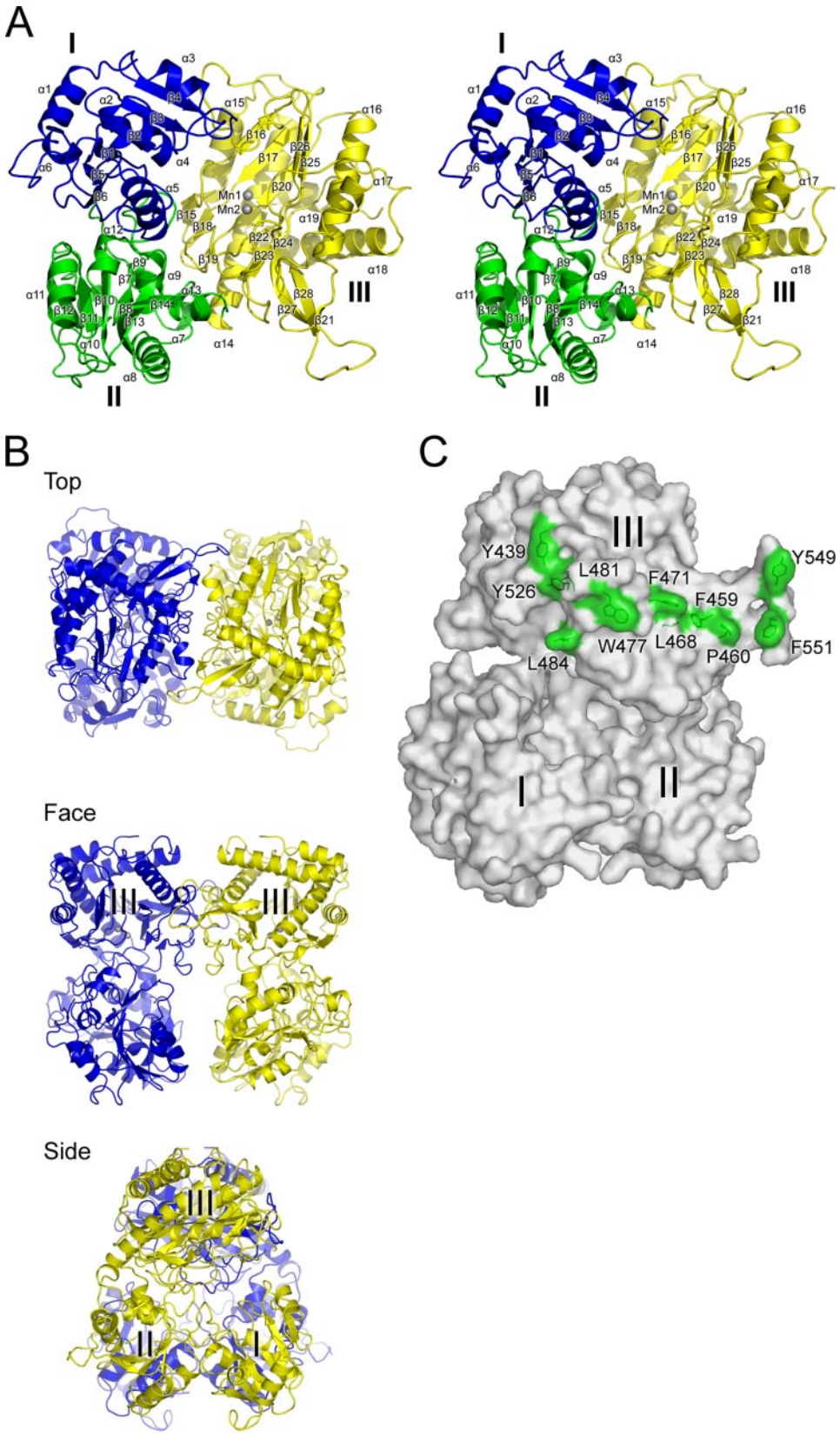

FIGURE 1. **Overall structure of XPNPEP1.** *A*, stereo view of a ribbon diagram of the XPNPEP1 monomer. Domain I (N-terminal domain) is colored *blue*, domain II (middle domain) is colored *green*, and domain III (C-terminal domain) is colored *yellow*. Mn^{2+} ions are shown as *gray spheres*. *B*, orthogonal views of the dimer of XPNPEP1. The two subunits are colored *blue* and *yellow*, respectively. The *labels* in the *side view only* refer to the *yellow* subunit. *C*, surface illustration and hydrophobic residues in the dimer interface. The overall surface is colored *gray*, and the hydrophobic residues in the dimer interface are colored *green*. The three domains are labeled *I*, *II*, and III in all panels.

Bank (PDB) with access code 3CTZ. Crystallographic statistics are summarized in Table 1.

Monomer Structure—The crystal structure unveiled a novel three-domain subunit for XPNPEP1. It includes an N-terminal domain (domain I, residues 1–161), a middle domain (domain II, residues 162–322), and a C-terminal domain (domain III, residues 323–623) (Fig. 1*A*). Secondary structure elements in each domain were defined by the DSSP program (18) (supplemental materials Table S1). Domain I is composed of a six-stranded (strands β1-β6) mixed β-sheet flanked by six α-helices (helices α1–α6). The topological order of the β-sheet is β4-β3-β2-β1-β5-β6, where strand β2 points in the opposite direction from the rest. Four helices (α1, α2, α3, and α6) are localized on one side of the sheet, and the remaining two (α4 and α5) on the other. The structure of domain II is similar to that of domain I. The core of domain II is also made up of a six-stranded (strands β8 and β10–β14) mixed β-sheet flanked by six α-helices (helices α8–α13). In addition, domain II contains a small antiparallel β-sheet (β7 and β9) and a short helix (α7) outside the core. Fig. 2*A* shows the result of secondary-structure matching superposition (19) between domains I and II, with 118 residues aligned to give a root mean square deviation of 2.6 Å. The two domains are related by a pure rotation of 150°. Domain III contains one strongly curved five-stranded antiparallel β-sheet (sheet I, β16-β17-β20-β26-β25), and two additional antiparallel β-sheets (sheet II, β15-β18-β19, and sheet III, β23-β22-β24-β27-β28-β21). On the outer face of the three sheets lie six α-helices (α14–α19). Of these, helices α14–α17 are oriented roughly parallel to the strands in sheet I, and α18 and α19 are near-perpendicular to the former helices. Strands β27 and β28 form a short hairpin structure that protrudes from the core.

Domains I and II are primarily held together by hydrophobic interactions. Domains II and III are

TABLE 1
Crystallographic data and refinement statistics

Statistic	Native	Peak	Edge	Remote
Data collection				
Space group				
$C222_1$				
Unit-cell parameters (Å)				
$a = 71.4$				
$b = 131.4$				
$c = 169.1$				
Wavelength (Å)	1.0000	0.9792	0.9794	0.9600
Resolution range (Å)	19.6−1.6	20−3.5	20−3.5	20−3.5
Measured reflections	741,394	75,366	75,172	74,950
Unique reflections	104,753	10,424	10,423	10,417
Completeness (%)	99.0 (95.8)	100 (100)	100 (100)	100 (100)
R_{merge} [a]	0.039 (0.209)	0.076 (0.098)	0.077 (0.102)	0.081 (0.113)
Redundancy	7.1 (6.4)	7.2 (7.1)	7.2 (7.1)	7.2 (7.0)
I/σ	47.1 (6.7)	32.3 (14.6)	30.3 (13.3)	28.4 (11.3)
Refinement				
R_{cryst} [b]/No. of ref. used		0.154/98,520		
R_{free} [c]/No. of ref. in test set		0.196/5,155		
Number of ion atoms		4		
Number of water molecules		1,055		
Overall figure of merit		0.88		
Root mean square deviation				
Bond length (Å)		0.011		
Bond angles (degrees)		1.28		
Average B factor (Å^2)		27.2		
Ramachandran plot (%) [d]		96.84/2.81/0.35		

[a] $R_{merge} = \Sigma_h\Sigma_i|I_i(h) - \langle I(h)\rangle|/\Sigma_h\Sigma_i\langle I_i(h)\rangle$, where $I_i(h)$ is the intensity of an individual measurement of the reflection, and $\langle I_i(h)\rangle$ is the mean intensity of the reflection.
[b] $R_{cryst} = \Sigma(||F_{obs}| - |F_{calc}||)/\Sigma|F_{obs}|$, where F_{obs} and F_{calc} are the observed and calculated structure-factor amplitudes, respectively.
[c] R_{free} was calculated as R_{cryst} using the reflections in a test set not used for structure refinement, which is a randomly selected subset containing 5% of unique reflections.
[d] Calculated using MolProbity. Numbers reflect the percentage of residues in the preferred, allowed, and disallowed regions, respectively.

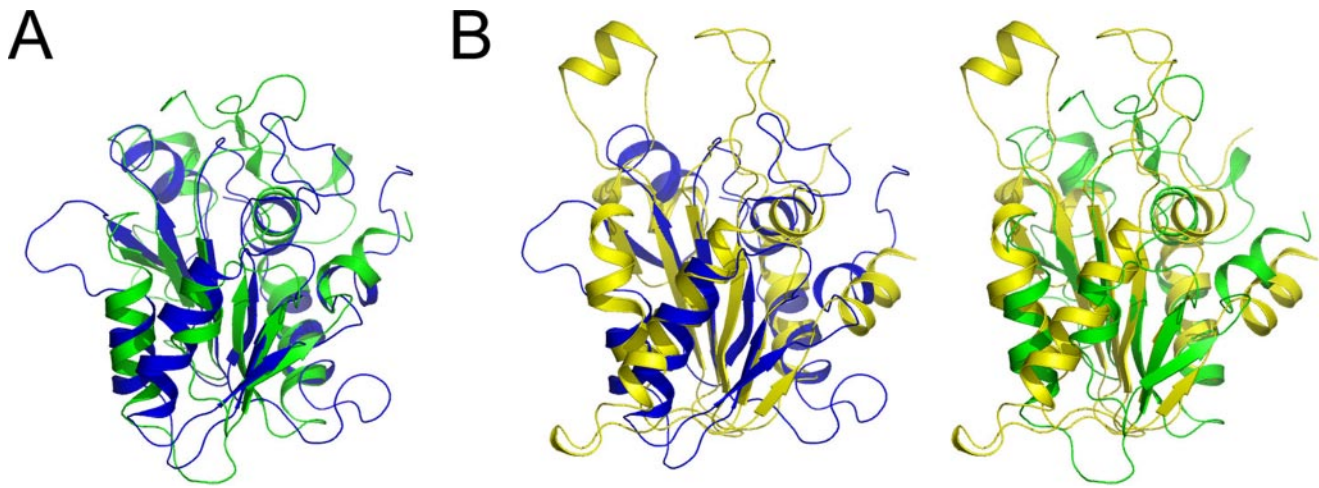

FIGURE 2. **Domain comparison.** *A*, comparison of domain I (*blue*) and domain II (*green*) from XPNPEP1. *B*, comparison of domain I (*blue*) or domain II (*green*) from XPNPEP1 (*yellow*) with the N-terminal domain from *E. coli* aminopeptidase P (*yellow*). Structures are shown in ribbon representation.

linked by the residues between helix α13 and helix α14 (residues 321–323).

Homodimer—Our solution studies, including gel filtration and AUC, revealed that XPNPEP1 proteins primarily exist as 140-kDa dimers (Fig. 3), which is consistent with previous reports (3, 4). In the crystal structure, two symmetry-related XPNPEP1 molecules (named as subunits A and B) are related by a dyad to form a homodimer (Fig. 1*B*). The two subunits are mainly held together by hydrophobic interactions (Fig. 1*C*). The side chains of Tyr^{439}, Leu^{481}, Leu^{484}, and Tyr^{526} in subunit A and Tyr^{549}, Phe^{551} in the β27–β28 hairpin of subunit B form one hydrophobic core. The symmetry equivalent hydrophobic residues form the second hydrophobic core of the dimer interface. Residue Pro^{460} and the side chains of Phe^{459}, Leu^{468}, Phe^{471}, and Trp^{477} in subunit A, together with their symmetry equivalents, form a third hydrophobic core. In addition to these hydrophobic interactions, a salt bridge between Glu^{442A} (*i.e.* Glu^{442} of subunit A) and Lys^{548B} and their symmetric counterparts, together with two pairs of hydrogen bonds between $Glu^{442A/B}$ and $Tyr^{549B/A}$, and between $Leu^{467A/B}$ and $Ser^{470B/A}$, also help to stabilize the interaction between the two subunits. Approximately 1,600 Å^2 (6%) of the solvent accessible surface area from each subunit is buried upon dimer formation. Among the above discussed residues, Trp^{477} plays a vital role for dimerization. Mutating this Trp to Glu abolished the capability of the enzyme to form a native dimer in our AUC studies (Fig. 3). Nevertheless, a small peak appeared at the position of 120 kDa in the AUC studies on the W477E mutant. We speculate that it represents a fraction of monomer or dimer with abnormal molecule shapes.

Active Site—The putative active site is located in the inner (concave) surface of the curved β-sheets of domain III (Fig. 1*A*) on the basis of comparison with homologous structures, such as the structure of *E. coli* AP-P (20–22). Two well coordinated metal ions were observed in this active site (Fig. 4). ICP-MS data consistently indicated that the molar ratio between Mn^{2+} and the 70-kDa XPNPEP1 subunit was 1.79:1, whereas the content of other common metals was negligible (Table 2). Although our crystallized XPNPEP1 protein sample was expressed with manganese-rich LB media and appeared clear, we carried out similar expression of the protein in plain LB media (*i.e.* without manganese supplementation) and interestingly obtained some "red protein." ICP-MS analysis on this red protein sample indicated that the protein contains mainly iron (0.73:1), manganese (0.70:1), and magnesium (0.41:1) ions (Table 2). Therefore, the molar ratio between the total metal ion content and the protein remained close to 2:1.

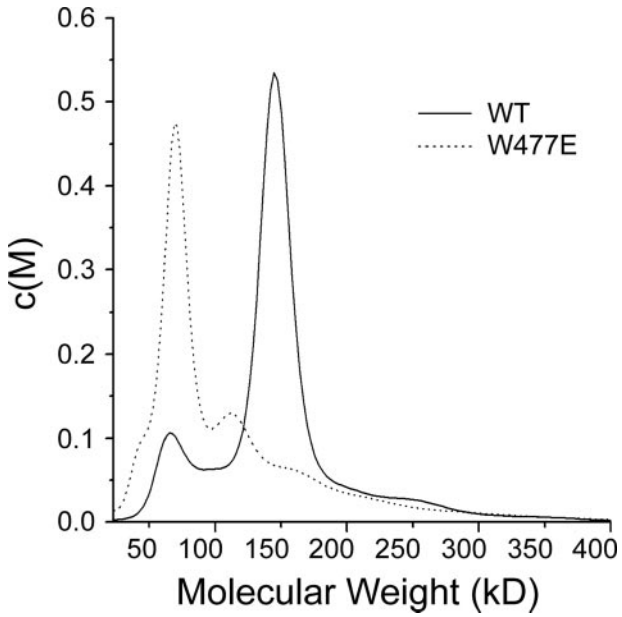

FIGURE 3. **AUC results for wild type XPNPEP1 (WT) and W477E mutant.** The AUC results are presented as a c(M) distribution model. The *solid curve* refers to wild type XPNPEP1 (WT), and the *dot curve* refers to the W477E mutant.

In our crystal structures, both Mn^{2+} ions are well coordinated. One of the Mn^{2+} ions (termed Mn1, see Fig. 4) is coordinated by the Oδ-1 atoms of Asp^{415} (2.15 Å) and Asp^{426} (2.14 Å), the Oϵ-1 atom of Glu^{537} (2.19 Å), and two water molecules (termed W1 and W2) with Mn^{2+}-ligand distances of 2.23 and 2.27 Å, respectively. These Mn^{2+}-ligands form an approximate trigonal-bipyramidal coordination geometry, with the Oδ-1 atoms of the two aspartate residues and W1 in the equatorial plane, and the Oϵ-1 atom of the glutamate residue and W2 on the axis. The coordination sphere of the second Mn^{2+} ion (termed Mn2) is comprised of the Oδ-2 atom of Asp^{426} (2.37 Å), the Oϵ-2 atoms of Glu^{523} (2.27 Å) and Glu^{537} (2.26 Å), Nϵ-2 atom of residue His^{489} (2.27 Å), and two water molecules (W1, 2.31 Å and W3, 2.17 Å), which complete a distorted octahedral coordination. Furthermore, W1 and the carboxylate groups of Asp^{426} and Glu^{537} act as bridges between the two Mn^{2+} ions. The side chains of His^{395}, His^{485}, His^{498}, and Glu^{41} surrounding the two Mn^{2+} ions are likely to play roles in recognition and catalysis during the substrate hydrolysis, according to studies on the equivalent residues in the active site of *E. coli* AP-P (22), which shares an almost identical active site with XPNPEP1.

Activity Assay—Activity assays on the same enzyme protein sample used for the crystallization were performed with the tripeptide Arg-Pro-Pro and bradykinin as substrates. The assays were performed in Mn^{2+}-free buffer and gave a K_m value of 308 (±8) μM and a k_{cat} of 7.7 s^{-1} on Arg-Pro-Pro, whereas K_m was measured as 78 (±9) μM and k_{cat} as 3.8 s^{-1} for bradykinin. Our K_m and k_{cat} values on bradykinin were comparable with previous reports (3, 5). Meanwhile, the red enzyme (enzyme expressed from plain LB) showed 44% activity of the Mn^{2+}-bound enzyme, and the activity of the enzyme dropped to 10% after treatment with 50 mM EDTA.

Although not directly involved in metal binding, Glu^{41} is the only residue located outside of the catalytic domain but close to the active site in the three-dimensional structure (Fig. 4). To test its function in catalysis, we made a mutant substituting Glu^{41} with Ala. This mutant maintained 91% of the WT activity, suggesting that it only marginally affects the activity of the enzyme. In contrast, another mutant, W477E, designed to block dimer formation and a domain I truncation mutant showed only 6 and 2% of the WT activity, respectively (Fig. 5).

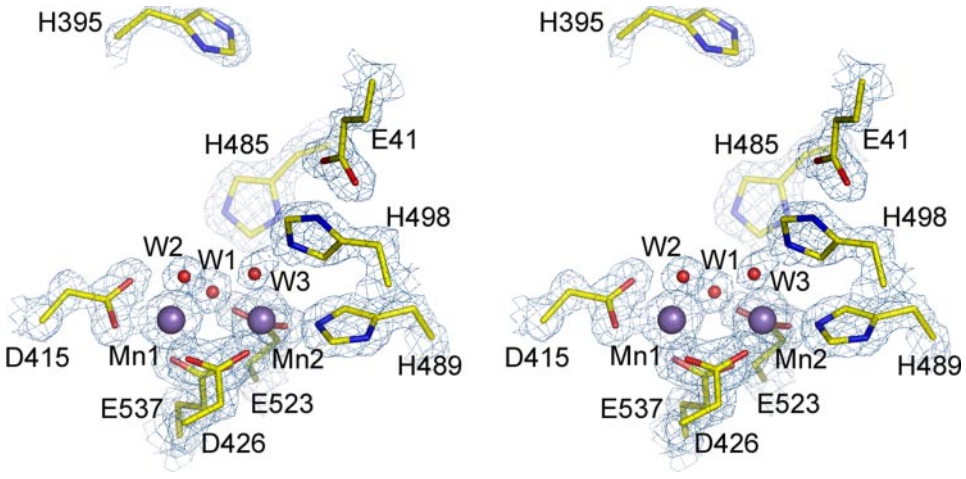

FIGURE 4. **Stereo view of the active site of human XPNPEP1 superimposed with a $2F_o - F_c$ electron density map contoured at 2σ.** Residues are colored by atom types (carbon in *yellow*, oxygen in *red*, and nitrogen in *blue*). Mn^{2+} ions and water molecules are shown as *gray* and *red spheres*, respectively.

DISCUSSION

XPNPEP1 Contains Two Mn^{2+} Ions in the Active Site—Prior to our structural study, Cottrell and colleagues (3) had reported some significant work on the characterization of recombinant XPNPEP1. In particular, they assayed the effects of different metal ions and chelating agents on the activity of XPNPEP1,

TABLE 2
Metal content of XPNPEP1 expressed from different media

Expression condition	Molar ratio between metal and protein[a]			
Manganese-rich LB media[b]	Magnesium	Calcium	Manganese	Iron
	0.012 ± 0.002	0.017 ± 0.004	1.791 ± 0.006	0.019 ± 0.003
	Co	Copper	Zincn	Total
	ND[c]	0.002	0.010	1.851 ± 0.015
Plain LB media	Magnesium	Calcium	Manganese	Iron
	0.409 ± 0.006	0.020 ± 0.001	0.698 ± 0.014	0.730 ± 0.011
	Cobalt	Copper	Zincn	Total
	ND	0.017	0.040 ± 0.001	1.914 ± 0.033

[a] The results are the mean of triplicate assays, and the amount of protein was regarded as 1. Standard deviations less than 0.0005 are not presented.
[b] Manganese-rich LB media was plain LB media with addition of $MnCl_2$ salt, to a final concentration of Mn^{2+} 1 mM.
[c] ND means no signal was detected.

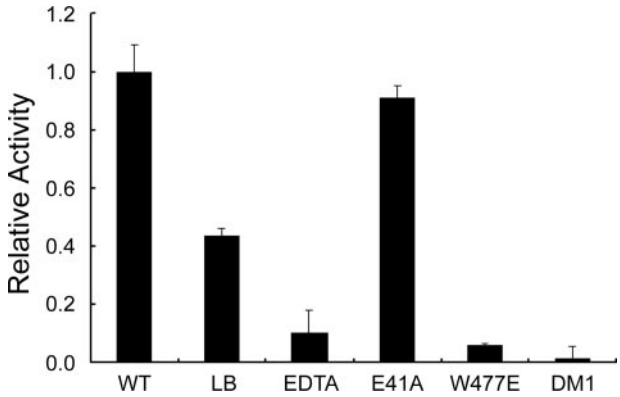

FIGURE 5. **Relative activities of XPNPEP1 expressed from manganese-rich LB (*WT*), from plain LB (*LB*), and treated with 50 mM EDTA (*EDTA*).** Also shown are the relative activities of the E41A mutant, W477E mutant, and domain I truncation mutant (*DM1*). The three mutants were all expressed from manganese-rich LB media. All samples were dialyzed against a buffer of 100 mM Tris-HCl (pH 8.0) and 100 mM NaCl prior to the activity assay. The tripeptide Arg-Pro-Pro was used as the substrate. Enzyme activities were normalized to the activity of the wild type enzyme expressed from manganese-rich LB (*WT*). The results are the mean of triplicate assays, and *error bars* represent standard deviations.

and identified the enzyme as Mn^{2+} dependent for its activity. It was based on this observation that we chose manganese-rich LB in our experiments to avoid Mn^{2+} depletion during protein expression. Nevertheless, their conclusion that each 70-kDa XPNPEP1 subunit contains only one metal ion was markedly different from the observation in our XPNPEP1 structure. The XPNPEP1 crystal structure displays two well coordinated metal ions with very strong electron density in each active site. The electron density map for the two metal ions can be observed even when contoured at the level of +20 standard deviations. To further investigate the metal content of the enzyme, an ICP-MS analysis on the XPNPEP1 recombinant protein expressed from manganese-rich LB was performed and revealed that the enzyme contains 1.79 Mn^{2+} ions per 70-kDa subunit and much lower levels of other metals. This result indicates the molar ratio between Mn^{2+} and the enzyme is nearly 2:1, which is entirely consistent with our structural observation. To study the effects of Mn^{2+} from the cell culture medium on the metal content of recombinant XPNPEP1, we expressed the enzyme in plain LB medium following the method of Cottrell and colleagues (3). ICP-MS analysis of this sample revealed three major metal contents, *i.e.* magnesium, manganese, and iron ions in the enzyme with the molar ratio 0.41, 0.70, and 0.73 per 70-kDa subunit. Although the molar ratio between Mn^{2+} and protein dropped to a level comparable with the previous report (0.99:1), the molar ratio between the total metal content and protein remains nearly 2:1, which is consistent with our structural observation. The detailed differences in metal content between our study and that of Cottrell *et al.* (3) may be due to different expression conditions, including temperature and induction time. For example, we used a "slow" expression method at 16 °C for 20 h. In contrast, their method was a quick one at 40 °C for 3 h. We believe that slow cell growth allows the recombinant protein to fold properly and to obtain the optimum metal ion content. Moreover, in our case, the difference in metal composition between XPNPEP1 samples expressed from plain and manganese-enriched LB medium was probably caused by the depletion of Mn^{2+} in the former, because the protein yields from both media were as high as 30 mg/liter of *E. coli* culture.

The Mn^{2+} content of XPNPEP1 expressed from plain LB was 39% (0.70:1.79) of that from manganese-rich LB and is fairly close to their activity ratio (44%). This suggests that only the portion of XPNPEP1 in which two Mn^{2+} ions are coordinated possesses catalytic activity, whereas the remaining portion, which coordinates either two magnesium or iron ions, presents little or no catalytic activity. Here, we made an assumption that XPNPEP1 preferentially binds the same type of ions in the two metal-binding sites, based on available structural evidence. Alternatively, Mn^{2+} is essential only for one of the two metal-binding sites; the other one is more tolerant to miscellaneous binding. Such a possibility remains to be further verified. Meanwhile, our result is comparable with previous data on the effect of divalent cations (3). Treatment of XPNPEP1 with EDTA greatly reduced its catalytic activity, both in our results and those of Cottrell and colleagues (3). We conclude that XPNPEP1 is a member of the double metal ion-dependent X-prolyl aminopeptidase, and coordinating two Mn^{2+} ions in its active site is most favorable for its activity.

X-prolyl Peptidases Have a Conserved Active Site and Catalytic Mechanism—Results from a BLAST search against the PDB sequences in the NCBI data base revealed weak sequence conservation between domain III of XPNPEP1 and the catalytic domains of other X-prolyl peptidases, including *E. coli* AP-P (PDB code 1wl9), X-prolyl dipeptidases (prolidase) from *Pyrococcus furiosus* (1pv9), prolidase from *Pyrococcus horikoshii* OT3 (1wy2), and human prolidase (2iw2). In contrast, no significant sequence homology is found for the two XPNPEP1 N-terminal domains (domain I and II). Sequence alignment of the conserved catalytic domain regions of these X-prolyl peptidases, together with the corresponding region of human XPNPEP2 revealed 11% identity and 38% similarity for the enzymes (Fig. 6). Although the sequence homology among these X-prolyl peptidases is marginal, residues for chelating metal ions are absolutely conserved in all six listed enzymes.

Superposition of structures of the five available active sites shows that there is a close agreement between the coordination geometries (Fig. 7). The ligand residues (*i.e.* Asp^{415}, Asp^{426}, His^{489}, Glu^{523}, and Glu^{537}) and most of the second shell of surrounding residues (*e.g.* His^{395}, His^{485}, and His^{498}) are conserved in both primary and three-dimensional structures.

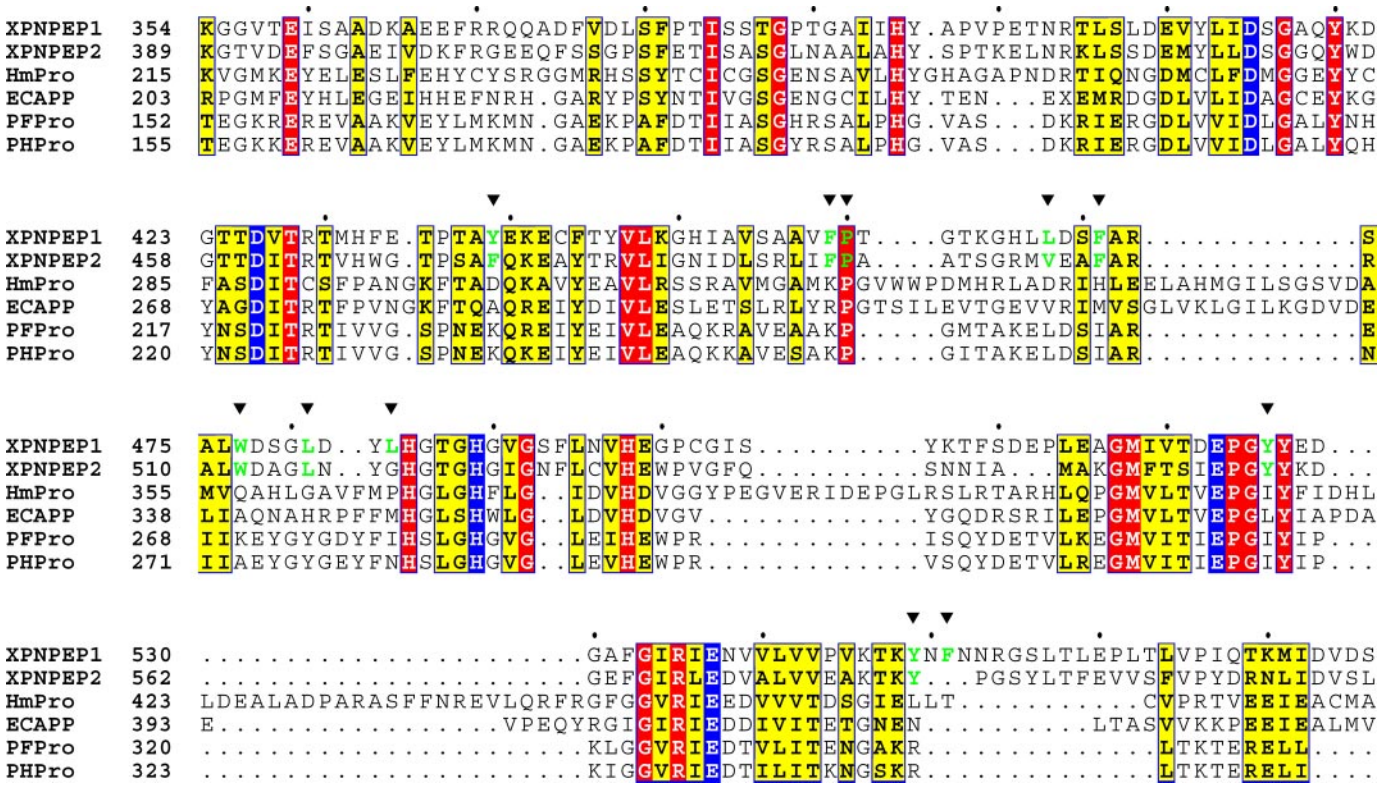

FIGURE 6. **Multiple sequence alignment of catalytic domains from X-prolyl peptidases.** From top to bottom, the sequences are from human XPNPEP1, human XPNPEP2 (GenBank™ number NP_003390), human prolidase (PDB code 2iw2), aminopeptidase P from *E. coli* (PDB code 1a16), prolidase from *P. furiosus* (PDB code 1pv9), and prolidase from *P. horikoshii* OT3 (PDB code 1wy2). Residues for chelating metal ion are highlighted with a *blue background*; other identical residues with a *red background*; and conserved residues with a *yellow background*. Hydrophobic residues on the dimer interface of XPNPEP1 and their equivalent residues on XPNPEP2 are colored *green*. The conserved region was defined by NCBI BLAST. Sequences were aligned using the program ClustalX, and the alignment was presented using the online ESPript server.

Among these X-prolyl peptidases, both human XPNPEP1 and *E. coli* AP-P are X-prolyl aminopeptidases (EC 3.4.11.9) with the same substrate specificity, and their activities require Mn^{2+} ions. The two Mn^{2+} ions in both XPNPEP1 and *E. coli* AP-P are five-coordinated (Mn1) and six-coordinated (Mn2), respectively, with the same amino acid ligands in the two structures. Superposition of the active site of XPNPEP1 with that of *E. coli* AP-P in complex with a product Pro-Leu dipeptide (PDB code 1a16, Fig. 7*A*) reveals that the positions of the Mn^{2+} ions, all ligand residues, and water molecules are identical. Only the side chain of His^{395} in XPNPEP1 exhibits a minor change from the equivalent His^{243} in *E. coli* AP-P. The structure and catalytic mechanism of *E. coli* AP-P have been extensively studied (20–22). Based on the close similarity of the active sites between XPNPEP1 and *E. coli* AP-P, they likely share the same catalytic mechanism. In *E. coli* AP-P His^{243} is proposed to form a hydrogen bond with the carbonyl of the proline residue in the substrate to stabilize its binding at the active site. The side chain of the corresponding His^{395} in XPNPEP1, which shows a higher temperature factor than the other active site residues and a non-functional rotamer, may regain its active conformation upon substrate binding.

In XPNPEP1, the Oϵ-1 atom on the side chain of Glu^{41} forms a hydrogen bond with the Nδ-1 atom of His^{498}. Thus, the side chain of Glu^{41} points toward the active site. Equivalent residues can be found in *E. coli* AP-P (Asp^{38} and His^{361}, Fig. 7*A*). In a previous study of *E. coli* AP-P, mutation of His^{361} to Ala caused Asp^{38} to change its χ_1 rotamer and move away from the active site (22). These data provide evidence that an interaction exists between the two residues, and it was consequently hypothesized that the imidazole ring of His^{361} can be doubly protonated by the carboxylate group of Asp^{38}. However, in our study of XPNPEP1, substitution of Glu^{41} with Ala did not significantly reduce its activity (Fig. 5), indicating that Glu^{41} is dispensable for the activity. Thus, its role in double protonation remains to be verified. Interestingly, both of the two prolidases from archaeobacteria species lack a residue equivalent to Glu^{41} in XPNPEP1 (Fig. 7*B*), arguing from a different perspective that this acidic residue is dispensable for catalytic activity.

XPNPEP1 Has a Novel Three-domain Structure—Although sequence alignment and structure superposition reveal that XPNPEP1 shares a conserved catalytic C-terminal domain and active site with other X-prolyl peptidases, it features a novel overall structure that distinguishes it from other known members of the X-prolyl peptidase family. Although all other X-prolyl peptidases were found to have only two domains in each subunit, namely one N-terminal domain and one C-terminal catalytic domain, XPNPEP1 uniquely contains three domains in each subunit: an N-terminal domain, a middle domain, and a C-terminal catalytic domain (Fig. 1*A* and supplemental materials Fig. S1, *top panel*). Comparing the XPNPEP1 subunits with those of the canonical X-prolyl peptidases, we discovered that domains II and III of XPNPEP1, respectively, occupy positions similar to the two domains in the canonical

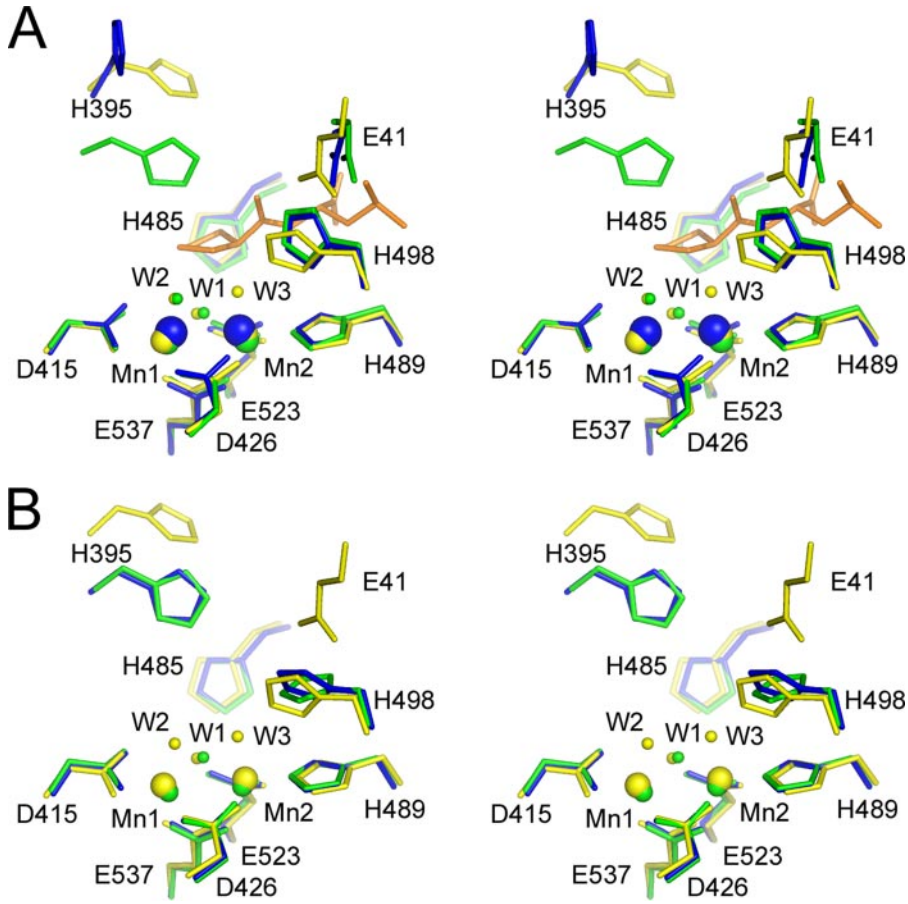

FIGURE 7. **Active site comparison with other X-prolyl peptidases.** *A*, stereo view showing the superposition of active sites from XPNPEP1 (*yellow*) and *E. coli* AP-P (*green*, PDB code 1a16) in complex with a product Pro-Leu dipeptide (*orange*) and human prolidase (*blue*, 2iw2). *B*, stereo view showing the superposition of active sites from XPNPEP1 (*yellow*) and prolidases from *P. furiosus* (*green*, 1pv9) and *P. horikoshii* OT3 (*blue*, 1wy2). Only the residues and atoms from XPNPEP1 are labeled.

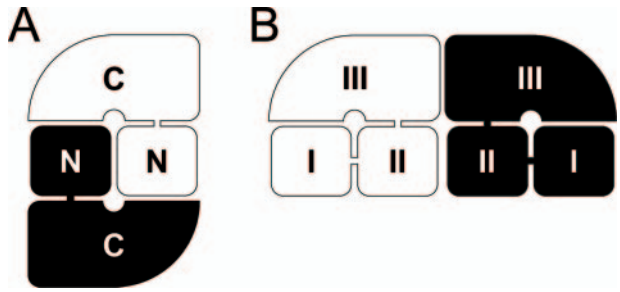

FIGURE 8. **Schematic diagram of X-prolyl peptidase dimerization.** *A*, model for the canonical X-prolyl peptidase dimers. *N* and *C* are labels for their N-terminal and C-terminal domains, respectively. *B*, model for the XPNPEP1 dimer. The three domains are labeled as *I*, *II*, and *III*. The two subunits in both *A* and *B* are colored *black* and *white*, respectively.

X-prolyl peptidase dimer. However, domain I in XPNPEP1 appears to be additional. As described above, Glu[41] is the only residue in domain I that interacts with the active site residues, yet it plays only a marginal role in catalysis, such that domain I appears not to participate in catalysis. However, our activity assays for a domain I truncation mutant of XPNPEP1 showed almost no catalytic activity (Fig. 5), indicating a crucial role of this domain. To investigate a possible role of this domain, we made a comparison between the XPNPEP1 subunit and canonical X-prolyl peptidase dimers (3, 20, 23, 24) (*e.g.* the *E. coli* AP-P dimer, which has 2100-Å^2 solvent accessible surface buried in the dimer interface). The position of domain I of XPNPEP1 is comparable with the positions of neighboring N-terminal domains in canonical X-prolyl peptidase dimers, and is especially similar to the two prolidases from archaeobacteria species (supplemental materials Fig. S1). Further superposition of XPNPEP1 domains I and II reveals that their core regions are similar (Fig. 2*A*). Superposition of domains I or II with the N-terminal domain of *E. coli* AP-P (Fig. 2*B*; 2.74 Å root mean square deviation for 124 residues between domain I and the N-terminal domain of *E. coli* AP-P, and 2.41 Å root mean square deviations for 107 residues between domain II and the N-terminal domain of *E. coli* AP-P) and other X-prolyl peptidases all indicate structure similarities in their core regions, albeit with no obvious sequence homology. Interestingly domains I and II in XPNPEP1 are related by a pure rotation of 150°, which is similar to but distinct from the dyad symmetry relationship between the two N-terminal domains in canonical X-prolyl peptidase dimers. These observations provide hints that a role of domain I in XPNPEP1 is, at least partially, to mimic the neighboring N-terminal domains in canonical X-prolyl peptidases dimers, so that the enzyme can maintain its active site pocket (Fig. 8).

Although all X-prolyl peptidases, including XPNPEP1, can form symmetrical homodimers, the dimerization of XPNPEP1 is different from those previously reported. In particular, the two XPNPEP1 subunits are arranged parallel to each other, whereas they are nearly perpendicular to each other in the canonical X-prolyl peptidase dimer (Figs. 1*B* and 8, and supplemental Fig. S1, *lower panel*). Although structural comparison between an XPNPEP1 subunit and other X-prolyl peptidase dimers suggest an isolated XPNPEP1 subunit might have full activity, our dimer blocking mutant of XPNPEP1, W477E, exhibited little catalytic activity (Fig. 5). We speculate that dimerization of XPNPEP1 plays a significant role in maintaining the correct fold of the enzyme. Interestingly, in all the other X-prolyl peptidases, each active site pocket is directly opened to solvent. However, in the case of the XPNPEP1 dimer, the active site pocket in each protomer is opened toward the partner protomer (Fig. 1*B*, face view). The result is that substrates have to access the active site from the gap between the two subunits. This feature may endow XPNPEP1 with selectivity for its favored substrate. In our kinetic assays for the nine-residue sub-

strate bradykinin (sequence: Arg-Pro-Pro-Gly-Phe-Ser-Pro-Phe-Arg) and its N-terminal tripeptide substrate Arg-Pro-Pro, XPNPEP1 showed a K_m for bradykinin almost four times smaller than the K_m for Arg-Pro-Pro. The stronger binding for the longer peptide substrate suggests the presence of additional binding sites that help its N terminus to access the active site.

Different Substrate Selectivity between X-prolyl Aminopeptidases and Prolidases May Be Due to Distinct Features of Their Active Site Pocket Entrance—All of the X-prolyl peptidases with published structures share nearly identical active sites, suggesting that they all share the same catalytic mechanism. However, X-prolyl aminopeptidases use long peptides with a penultimate proline residue as their substrate, whereas prolidases allow only X-Pro dipeptides. Comparing their active site pockets, we find that the pockets of X-prolyl aminopeptidases are shallow and wide. In contrast, the pockets of prolidases are much deeper and more twisted, such that long peptide substrates would be unable to reach their active sites.

The structure of *E. coli* AP-P in complex with a product Pro-Leu dipeptide molecule provides a good model for studying their different substrate selectivity on tripeptides among X-prolyl aminopeptidases (supplemental material Fig. 2*S*). From superposition of their active sites, no residue is found in XPNPEP1 that would have a steric conflict with the Leu residue of the Pro-Leu product. However, the side chain of Arg^{399} in human prolidase appears to largely occupy the position of the Leu residue in the dipeptide product, and thus the tripeptide substrate is predicted to be unfavorable as a substrate for the prolidase. Similarly, the side chains of Ser^{281} and Arg^{295} of prolidase from *P. furiosus* (Ser^{284} and Arg^{298} of prolidase from *P. horikoshii* OT3) may cause steric hindrance with the Leu residue of the product.

XPNPEP2 May Be Another Three-domain X-prolyl Aminopeptidase—Mammals are known to contain two X-prolyl aminopeptidases: one is cytosolic (XPNPEP1) and the other is membrane bound (XPNPEP2). The XPNPEP2 consists of an N-terminal signal peptide to direct its translocation into endoplasmic reticulum and a C-terminal glycosylphosphatidylinositol anchor sequence (10, 25). The human XPNPEP2 consists of 674 residues and shares 42% sequence identity and 61% positives with XPNPEP1. Aside from the active site residues, nearly all of the hydrophobic residues that contribute to dimerization in XPNPEP1 have their equivalent residues in XPNPEP2 (Fig. 6). Based on its size and sequence similarity with XPNPEP1, we predict that XPNPEP2 shares the same three-domain X-prolyl aminopeptidase fold and dimerization as XPNPEP1.

Both XPNPEP1 and XPNPEP2 can hydrolyze bradykinin containing a penultimate proline residue and are inhibited by the same specific inhibitor, apstatin (1–3). Bradykinin is a small vasoactive peptide involved in a variety of biological processes (26, 27). Experiments performed in mice *in vivo* showed that administration of apstatin can reduce myocardial infarction severity (11). Based on the structure of XPNPEP1, designing or screening for new chemical inhibitors for XPNPEP1 and XPNPEP2 may result in novel therapeutic approaches for the prevention of myocardial infarction.

Acknowledgments—We thank Dr. Chaoneng Ji from Fudan University, Shanghai, China, for kindly providing the XPNPEP1 gene; Zhongnian Zhou, Meirong Zhang, and Xiaoxia Yu for assistance with analytical ultracentrifugation and other assays at the Institute of Biophysics (IBP), Chinese Academy of Sciences.

REFERENCES

1. Prechel, M. M., Orawski, A. T., Maggiora, L. L., and Simmons, W. H. (1995) *J. Pharmacol. Exp. Ther.* **275,** 1136–1142
2. Lloyd, G. S., Hryszko, J., Hooper, N. M., and Turner, A. J. (1996) *Biochem. Pharmacol.* **52,** 229–236
3. Cottrell, G. S., Hooper, N. M., and Turner, A. J. (2000) *Biochemistry* **39,** 15121–15128
4. Rusu, I., and Yaron, A. (1992) *Eur. J. Biochem.* **210,** 93–100
5. Vanhoof, G., De Meester, I., Goossens, F., Hendriks, D., Scharpe, S., and Yaron, A. (1992) *Biochem. Pharmacol.* **44,** 479–487
6. Harbeck, H. T., and Mentlein, R. (1991) *Eur. J. Biochem.* **198,** 451–458
7. Gilmartin, L., and O'Cuinn, G. (1999) *Neurosci. Res.* **34,** 1–11
8. Dehm, P., and Nordwig, A. (1970) *Eur. J. Biochem.* **17,** 372–377
9. Simmons, W. H., and Orawski, A. T. (1992) *J. Biol. Chem.* **267,** 4897–4903
10. Hooper, N. M., Hryszko, J., and Turner, A. J. (1990) *Biochem. J.* **267,** 509–515
11. Wolfrum, S., Richardt, G., Dominiak, P., Katus, H. A., and Dendorfer, A. (2001) *Br. J. Pharmacol.* **134,** 370–374
12. Otwinowski, Z., and Minor, W. (1997) *Methods Enzymol.* **276,** 307–326
13. Terwilliger, T. C., and Berendzen, J. (1999) *Acta Crystallogr. Sect. D Biol. Crystallogr.* **55,** 849–861
14. Blanc, E., Roversi, P., Vonrhein, C., Flensburg, C., Lea, S. M., and Bricogne, G. (2004) *Acta Crystallogr. Sect. D Biol. Crystallogr.* **60,** 2210–2221
15. Emsley, P., and Cowtan, K. (2004) *Acta Crystallogr. Sect. D Biol. Crystallogr.* **60,** 2126–2132
16. Collaborative Computational Project, Number 4 (1994) *Acta Crystallogr. Sect. D Biol. Crystallogr.* **50,** 760–763
17. Schuck, P. (2000) *Biophys. J.* **78,** 1606–1619
18. Kabsch, W., and Sander, C. (1983) *Biopolymers* **22,** 2577–2637
19. Krissinel, E., and Henrick, K. (2004) *Acta Crystallogr. Sect. D Biol. Crystallogr.* **60,** 2256–2268
20. Wilce, M. C., Bond, C. S., Dixon, N. E., Freeman, H. C., Guss, J. M., Lilley, P. E., and Wilce, J. A. (1998) *Proc. Natl. Acad. Sci. U. S. A.* **95,** 3472–3477
21. Graham, S. C., Maher, M. J., Simmons, W. H., Freeman, H. C., and Guss, J. M. (2004) *Acta Crystallogr. Sect. D Biol. Crystallogr.* **60,** 1770–1779
22. Graham, S. C., Lilley, P. E., Lee, M., Schaeffer, P. M., Kralicek, A. V., Dixon, N. E., and Guss, J. M. (2006) *Biochemistry* **45,** 964–975
23. Endo, F., and Matsuda, I. (1991) *Mol. Biol. Med.* **8,** 117–127
24. Maher, M. J., Ghosh, M., Grunden, A. M., Menon, A. L., Adams, M. W., Freeman, H. C., and Guss, J. M. (2004) *Biochemistry* **43,** 2771–2783
25. Hyde, R. J., Hooper, N. M., and Turner, A. J. (1996) *Biochem. J.* **319,** 197–201
26. Regoli, D. (1983) *Adv. Exp. Med. Biol.* **156,** 569–584
27. Bhoola, K. D., Figueroa, C. D., and Worthy, K. (1992) *Pharmacol. Rev.* **44,** 1–80